Effect of propeller induced flow on the performance of biplane micro air vehicle dynamics

Journal Title
XX(X):1–10

DOI: 10.1177/ToBeAssigned
www.sagepub.com/
SAGE

Shuvrangshu Jana[1] **Harikumar Kandath**[1] **Mayur Shewale**[1] **M. Seetharama Bhat**[1]

Abstract

This paper presents the analysis of the propeller induced flow effects on the dynamics of a fixed wing biplane Micro Air Vehicle (MAV). The analysis is based on wind tunnel tests and mathematical modelling. This analysis plays a pivotal role because the propeller induced flow has significant effects on the dynamics of fixed wing MAV due to submergence of a large portion of the wing in propeller slipstream. Although the effect of propeller induced flow on the various aerodynamic parameter is reported in the literature; however, its effects on overall forces, moments and vehicle dynamics are not quantified so far. In this paper, propeller induced flow effects are modelled as a function of motor rotation speed and mathematical analysis is performed to quantify their effects. The wind tunnel test is conducted at different propeller speed on a biplane MAV "Skylark", having wingspan and chord length of 150 mm and 140 mm respectively. Analysis of results shows that propeller slipstream increases the overall lift, drag, side force, range, and endurance significantly. Propeller flow also contributes to rolling moment and pitching moment, while it has negligible effects on the yawing moment. It is shown that the trim angle of attack is lower when propeller flow is considered in computing the trim conditions.

Keywords

Propeller induced flow, Micro air vehicle, Modelling, Biplane, Fixed wing

Introduction

Micro Air Vehicles (MAVs) are soon becoming one of the essential assets in search and rescue, reconnaissance, surveillance missions and are also gaining importance in a tactical environment[1]. Specifically, the vehicle whose maximum dimension is less than 150 mm and velocity around 10 m/s belongs to the class of MAVs[2]. Amongst the various types of MAVs, fixed wing MAVs are superior as they are silent, offer more endurance, can carry a higher payload, fly faster and higher and are virtually undetectable.

Accurate modelling of vehicle dynamics is crucial for analyzing the stability and performance of the vehicle while performing a specific mission. As most of the wing is submerged in propeller slipstream, the propeller induced flow has a significant contribution to the total forces and moments acting on the MAV.

Propeller induced flow increases the kinetic energy of the free stream causing the flow of energy towards the downstream to be higher than the flow energy upstream of the propeller. The effect of propulsive force on the aerodynamics of wing for bigger size vehicles is reported in various open literature[3–7]. In general, propeller induced flow changes the lift curve slope, drag polar, and also affects the flow transition and flow separation due to the formation of a modified boundary layer; however, the effects of propeller induced flow to the overall aerodynamics of the vehicle is less for high aspect ratio wing and high Reynolds number flow.

MAVs are generally of low aspect ratio (AR) typically less than 2 and operated in low Reynolds number (typically 50000- 100000). In this region, the lift to drag ($\frac{L}{D}$) ratio reduces drastically due to the formation of a laminar separation bubble[8]. The size of the propeller dimension to the wing dimension is comparable in the case of propeller-driven MAV; hence, the effect of propeller induced flow on

[1] Department of Aerospace Engineering, Indian Institute of Science, India

Corresponding author:
Shuvrangshu Jana, Micro Air Vehicle Laboratory, Department of Aerospace Engineering, Indian Institute of Science, Bengaluru-560012, India

Email: shuvra.ce@gmail.com

the overall aerodynamics is quite significant as it influences the flow transition[9], flow separation, flow reattachment and formation of laminar separation bubbles[10]. The important parameters which are affected by the propulsive forces are stall angle of attack[11], lift coefficient (C_L) and drag coefficient (C_D)[12], the slope of lift versus angle of attack curve[13], $\frac{L}{D}$ ratio[14 15], pitching moment[17] etc. Propeller flow also influences the transition from laminar flow to turbulent flow[16]. The aerodynamic performance and stability of the MAV strongly depend on the flow behaviour generated from the propeller flow stream.

The behaviour and characteristics of flow around an object can be investigated through simulation as well as from wind tunnel tests[18–20]. The effects of propeller induced flow on the aerodynamics of small scaled vehicle is performed through Computational Fluid Dynamics (CFD) simulation[17,18,21–24] and also by conducting wind tunnel tests[10,11,14,15,25–27]. Wind tunnel test on MAV with a wingspan of 300 mm in Reynolds number range of 120000-180000 showed that propeller induced flow increase the lift coefficient at a higher angle of attack and delay the stall[11]. Similarly, experiments at Reynolds number 135000 with motor rotation in the range of 8000-10000 RPM with 300 mm wingspan model showed an increase of C_L at a higher angle of attack (AoA) and increase of C_D with propulsive flow[12]. The effects of propeller induced flow on C_L and C_D further increases with an increase in the speed of motor rotation. Similarly, the increase of lift, drag and stall AoA with increasing slipstream to free stream velocity ratio is observed during wind test on a model with a wingspan of 252.0 mm and a chord length of 142.6 mm with a propeller diameter of 5.5 inches in the velocity range of 5-15 m/s[25].

A significant delay in stall and increase in slope of the lift versus angle of attack is observed with the propeller induced flow in the wind tunnel experiment on a flat plate with AR (2-4) at Reynolds number 60000-90000, and these quantities are found to increase with the increase in motor rotation rate[13]. In[10], wind tunnel test on a square planform wing having a span and chord length of 12 inches with a diameter of 8 inches in tractor configuration in the velocity range of 6-10 m/s and motor RPM of 6000-8000 also showed an increase in the slope of lift curve by 1-1.13 times due to prop-wash effects. In this case, the factor K of the induced drag is also reported to be 0.9-1.12 times due to propulsive flow.

In[22], dual-time preconditioning and overset grid methodologies are employed to simulate the influence of propeller flow. The increment of the aerodynamic coefficient, stall angle of attack and decrement of lift to drag ratio of MAV is observed due to propeller flow. In contrast, in the range of Reynolds number (30000-80000) and aspect ratio of the wing (2-5); the increment of $\frac{L}{D}$ ratio as high as 10-12 is reported due to increasing lift and reduction of pressure drag under the influence of propeller slipstream[14]. In another experiment, the decrease of $\frac{L}{D}$ ratio at a lower angle of attack and increase of $\frac{L}{D}$ ratio at a higher angle of attack due to the propeller slipstream is reported for the wind tunnel test on 9 inches wingspan model in the range of Reynolds number range of $5 \times 10^4 - 1 \times 10^5$. The configuration of the flow source also affects significantly the dynamics of flow[28]. Computational investigation of flow around Reynolds number 83000 showed that tractor configuration increases the $\frac{L}{D}$ ratio slightly and pusher configuration decreases the $\frac{L}{D}$ ratio. Similarly, the increment of pitching moment[17] and slope of pitching moment curve[29] due to propeller induced flow is reported in[17].

The vehicles used in the above-mentioned literature are monoplanes having a wingspan exceeding 150 mm. Although the effects of propulsive flow on the individual parameters are discussed in the above experiments, the effects on the overall system dynamics are not reported. In[30], the non-linear model of the "KH2013A" MAV having span and chord length within 150 mm is developed incorporating the propeller rotation; however, the propeller rotation is not separately modelled and its effects on the aerodynamic performance are not analysed. In case of biplane configuration, the effect of propulsive flow due to different motor configurations on the aerodynamic efficiency of fixed wing biplane having AR equal to 1 and Reynolds number in the range of 55250-110500 is reported[31]. The propulsive configuration is found to be more efficient in terms of aerodynamic performance for the low-speed flight; however specific effect of propulsive induced flow is not analysed. As per the author's knowledge, the propeller slipstream effect on the aerodynamic parameters of fixed wing biplane is not reported so far in the open literature.

In this paper, the effects of propeller induced flow on the dynamics of a fixed-wing biplane MAV, called "Skylark", having a wingspan and chord length not exceeding 150 mm (AR=1.07) is analyzed around Reynolds number of 67000. Wind tunnel test of the biplane MAV "Skylark" is performed in free stream flow as well as with only propulsive flow at the different motor rotation rates in a tractor configuration. The mathematical model of the MAV is developed with and without propeller rotation to understand its effects on different aerodynamic parameters.

It is observed that the propeller induced flow increases the lift force, drag force, side force and add negative rolling,

pitching and yawing moment to the overall system. The novelty of the paper lies in the following aspects:

- Mathematical quantification of the contribution of propeller rotation toward overall forces and moments from wind tunnel experimental data.
- Analysis of propeller induced flow for a fixed wing biplane MAV.

The rest of the paper is organized as follows. Details of the specification of the fixed wing biplane MAV used for wind tunnel testing is described in **Vehicle parameters** section. In **Wind tunnel test** section, description of wind tunnel and test set up is discussed. The forces and moments acting on the vehicle due to propeller induced flow as well as free stream flow and their comparison are discussed in **Forces and moments** section. Section **Range and endurance** describes the effect of propeller induced flow on the range and endurance of the MAV. The relative contribution of force and moments due to the propeller rotation at a typical operating point of "Skylark" MAV are discussed in section **Trim point analysis**.

Vehicle parameters

The summary of the parameters of "Skylark" MAV (shown in Figure 1) is given in Table 1.

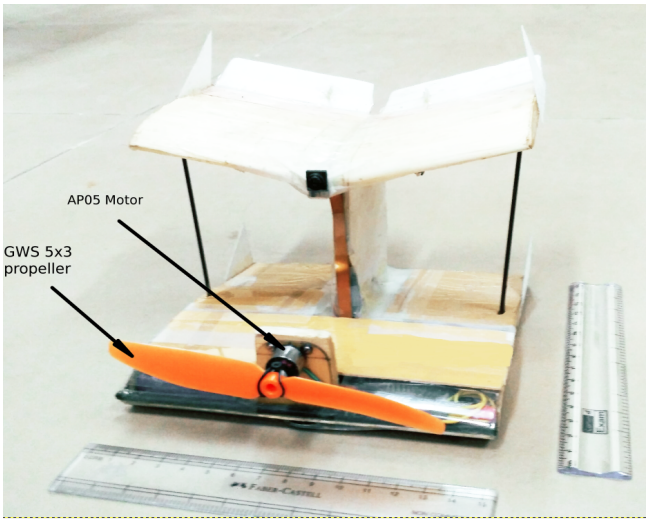

Figure 1. Photograph of "Skylark" MAV

The diameter of the propeller is 5 inches and the wingspan of MAV is 6 inches; clearly, most of the wing is affected by the propeller slipstream.

Velocity streamlines in case of propeller off condition at a nominal velocity of 8 m/s are shown in Figure 2. Different colours indicate velocity magnitude ranging from 0 to 11.9 m/s as shown in Figure 2. The magnitude of the velocity

Table 1. "Skylark" specifications.

Component	parameter	Value
Bottom wing	Span	150 mm
	Chord	140 mm
	Aerofoil	Modified MH-60
	Aerofoil thickness	12 %
	Planform	Rectangular
Top wing	Span	150 mm
	Chord	85 mm
	Aerofoil	Modified MH-60
	Aerofoil thickness	8 %
	Dihedral	12 degrees
Vertical tail	Area	80 mm $\times$ 60 mm
	Height	80 mm
Control surface (Elevon)	Size(each)	75 mm $\times$ 26 mm
Winglet	Size(each)	45 mm $\times$ 30 mm
Motor	Type	Micro brushless
	Brand	AP05 5000 kv
Propeller	Brand	GWS 5030
	Diameter	5 inches
	Pitch	3 inches
Surface material	Wing	Balsa sheet
	Vertical tail	Depron
	Control surface	Depron

streamlines goes up to a maximum of 11.9 m/s near to the motor mount. The flow visualization is performed through CFD analysis.

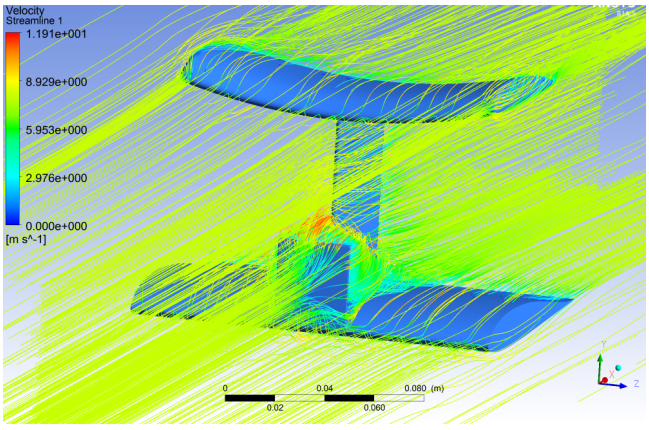

Figure 2. Velocity streamlines

Wind tunnel test

The wind tunnel test is performed in the Micro Air Vehicle Aerodynamics Research Tunnel (MART) at National Aerospace Laboratory (NAL) complex in India. The test is conducted in closed test sections in open circuit low-speed wind tunnel.

Tunnel description

The details of the wind tunnel geometry are given in Table 2. The schematic of wind tunnel is shown in Figure 3 .

Table 2. Wind tunnel geometry

Description	Specification
Test section	0.8 m × 1.2 m × 2.5 m
Contraction ratio	9:1
Tunnel length	17 m
Entry section	Bell shape with fitness ratio of 8
Type of honeycomb	Square cells
Turbulence screens	3 Nos.

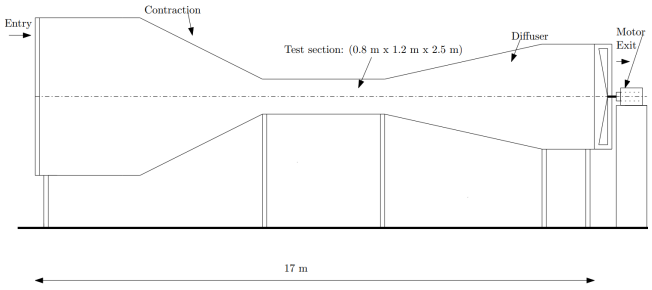

Figure 3. Schematic of wind tunnel used for testing the MAV

The mean flow velocity variation is observed in the range of -0.1- 0.1 %. The turbulence intensity level is observed to be within 0.1 % for velocity up to 10 m/s and within 0.15 % for velocity range 10-45 m/s. The forces and moments are measured using Mini40, which is an ATI six-axis force and torque sensor that measures outputting forces and torques from all three Cartesian coordinates (x,y,z). At each time, an average of 5000 measurements is taken as the measured value. These forces and moments are transformed to lift force, drag force, side force and moments along the body frame of "Skylark" for standard analysis. The possible range of important variables for the wind tunnel set up is mentioned in Table 3.

Table 3. Possible test condition

Description	Specification
Velocity range	1-45 m/s
Angle of attack	-4^o to 32^o
Angle of Side slip	-7^o to 7^o

The uncertainties in the measured data are expressed as the sum of fixed uncertainty due to the precision of load cells and an uncertainty proportional to the measured variable, expressed in percentage. The total uncertainty is expressed for the measurement obtained for a velocity of 8 m/s in the Table 4 below.

Table 4. Uncertainties at velocity of 8 m/s.

Quantity	Uncertainties
Lift force	1.0 grams + 6 %
Drag force	0.5 grams + 6 %
Rolling moment	1.25 gram-cm + 6 %
Pitching moment	1.25 gram-cm + 6 %
Yawing moment	1.25 gram-cm + 6 %

Test set up

The test is performed in the velocity range of 6-16 m/s and for the full range of angle of attack and angle of sideslip. The flying model of " Skylark" is mounted inside the tunnel section, as shown in Figure 4 and Figure 5.

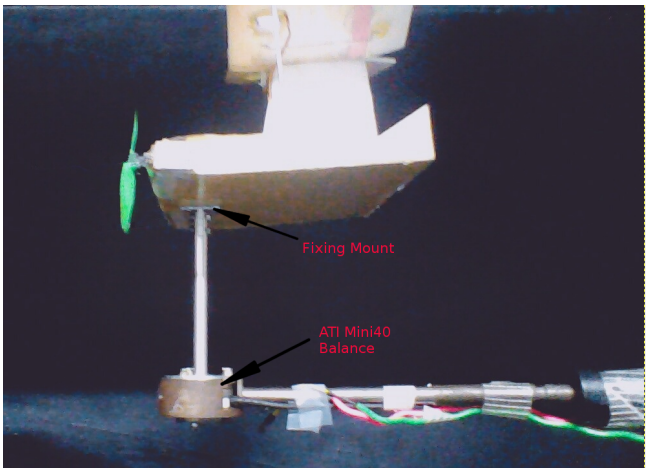

Figure 4. Mounting of MAV in windtunnel

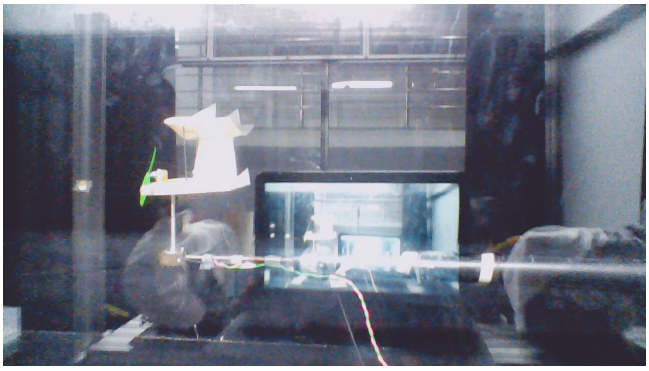

Figure 5. Snapshot of MAV in windtunnel

The wind tunnel set up allows the automatic setting of the different position of the angle of attack, sideslip and direct recording of the data from the balance sensor. Motor RPM is varied by varying the input throttle PWM. The test model is fitted with an autopilot with telemetry and a receiver. Throttle command is sent from a radio controller and received by the onboard receiver which then converts the command to an equivalent rotation speed command for the motor.

The input commands are transmitted to a ground station software using the telemetry port. The desired throttle PWM is maintained by observing the telemetry data at the ground station. The mapping between the motor RPM and the throttle PWM is developed beforehand using a tachometer. The similar technique is used to generate the control commands for varying the position of control surfaces.

Forces and moments

Details of the modelling of "Skylark" is discussed in[32]. In this paper, the forces and moments acting on the "Skylark" is discussed again for detailed analysis of the effect of propeller induced flow. In Figure 6, the different forces and moments acting on "Skylark" is shown as a schematic diagram.

Propeller induced flow has significant effects on the lift force, drag force, and pitching moment; whereas side force, rolling moment and the yawing moment is also affected due to the asymmetric flow distribution around the propeller. The side force and rolling moment due to propeller flow is quite significant if vertical surfaces like a vertical tail are placed in the propeller wash. A significant part of the rolling moment is also contributed from motor counter torque. Combined effects of propeller induced flow and motor counter torque on different forces and moments are modelled as a function of motor RPM.

Forces and moments are modelled separately due to free stream flow and due to the combined effect of propeller induced flow and motor counter torque. The static derivatives and control derivatives are measured using the wind tunnel test while the dynamic derivatives are measured using standard empirical results[33]. It is to be noted that during wind tunnel test all the forces and moments are measured in vehicle body frame. Lift and drag forces are generally expressed in the stability frame; so, lift and drag forces are modelled in stability frame for ease in standard interpretation. For modelling purpose, the angles are expressed in radian and angular rates are expressed in rad/s.

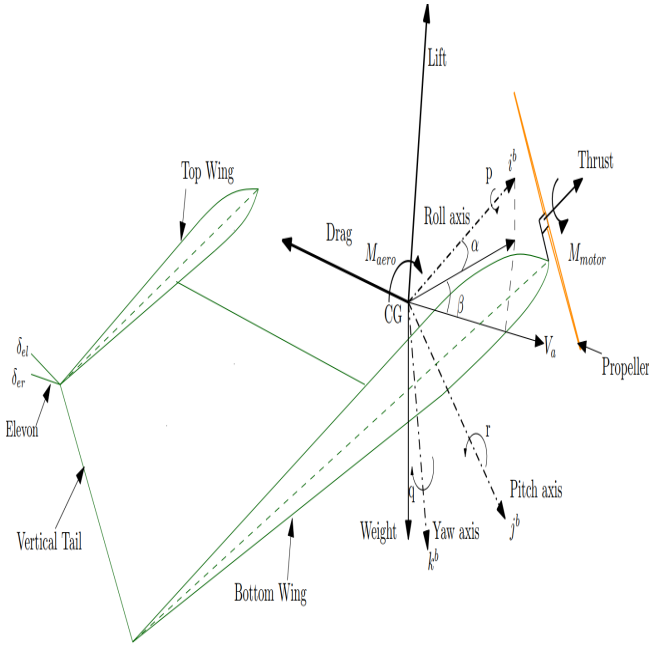

Figure 6. Diagram showing the axis convention, forces and moments acting on MAV

Lift and drag force

Lift and drag forces acting on MAV at any instant mainly depend on the elevator deflection (δ_e), vehicle angle of attack (α), pitch rate (q) and motor RPM (ω). Lift and drag forces are expressed in equations 2-6:

$$F_{Lift} = \frac{1}{2}\rho V_a^2 S\left(C_L(\alpha) + C_{L_q}\frac{c}{2V_a}q + C_L(\delta_e)\right) + f_L(\omega) \quad (1)$$

$$F_{Drag} = \frac{1}{2}\rho V_a^2 S\left(C_D(\alpha) + C_{D_q}\frac{c}{2V_a}q + C_D(\delta_e)\right) + f_D(\omega) \quad (2)$$

$$C_L(\alpha) = -0.065 + 2.9\alpha - 2\alpha^2 \quad (3)$$

$$C_D(\alpha) = 0.15 + 0.1\alpha + 1.5\alpha^2 \quad (4)$$

$$f_L(\omega) = 0.0022 - 4.6\delta_\omega + 11\delta_\omega^2 - 5.8\delta_\omega^3 \quad (5)$$

$$f_D(\omega) = -0.003466 + 15.86\delta_\omega - 52.19\delta_\omega^2 + 57.52\delta_\omega^3 - 21.01\delta_\omega^4 \quad (6)$$

where, $\delta_\omega = \dfrac{\omega + 9300}{22765}$.

In the above equations, $f_L(\omega)$, and $f_D(\omega)$ denotes the contribution of propeller flow to the lift and drag forces respectively. The expression for $f_L(\omega)$ and $f_D(\omega)$ are given in equations 5 and 6 respectively. The dynamic and control derivatives of the lift and drag force expression is mentioned in Table 5.

Table 5. Dynamic and control derivatives.

Dynamic	Value	Control	Value
C_{L_q}	1.1339	$C_L(\delta_e)$	0.92 δ_e
C_{D_q}	0	$C_D(\delta_e)$	$-0.06332\delta_e + 0.176\delta_e^2$

The variation of coefficient of lift only due to the propeller induced flow as a function of motor RPM is shown in Figure 7, here $C_L(\omega) = f_L(\omega)/(0.5\rho V_a^2 S)$. Clearly, the lift force increases with the motor rotation as it imparts more kinetic energy to the flow.

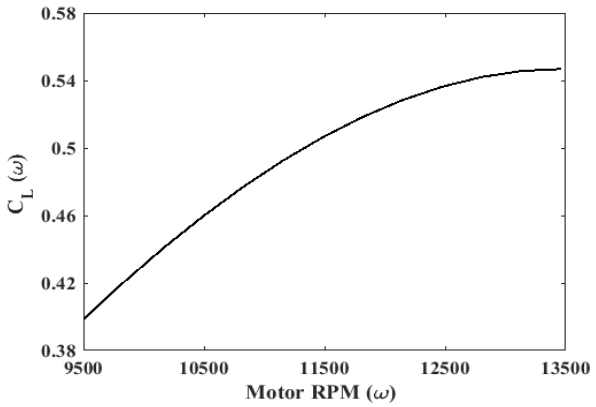

Figure 7. Lift coefficient vs Motor RPM

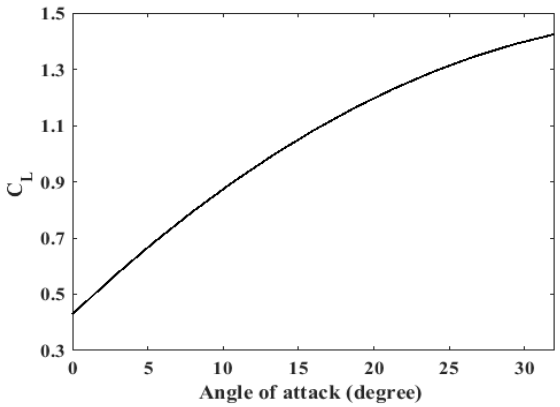

Figure 8. Total lift coefficient at 90 % throttle (Motor RPM=11200)

The exact values of pitch rate, elevator angle, motor rotation corresponding to a particular angle of attack are difficult to set up in wind tunnel. Due to free stream flow, the amount of lift produced by the angle of attack of vehicle consist of a major portion of the total lift, as the effect of pitch rate and elevator angle is comparatively low. For the analysis of the relative contribution of propeller induced flow towards the total lift; the effect of pitch rate and elevator angle is ignored. The exact contribution of propeller induced flow toward the total lift at a particular operating point is also analyzed at the end.

Figure 8 shows the variation of overall lift coefficient with angle of attack at the motor RPM of 11200, here $C_L = F_{Lift}/(0.5\rho V_a^2 S)$. In Figure 8, the free stream flow is considered as 8 m/s and the RPM value is approximately 90 % of the total throttle. At an angle of attack of 18^o and free stream flow of 8 m/s, the lift force at a different percentage of the throttle is tabulated in Table 6. At 90 % throttle, the lift force due to propeller induced flow is 54.40 grams and the total lift is 125.81 grams; therefore, propeller induced flow increases the lift force by 76.18 %. Clearly, in the case of small-scale vehicles lift force is strongly affected by the propeller induced flow.

Table 6. Lift at different percentage of throttle.

Throttle	RPM	Lift due to propeller induced flow (grams)	Total lift (grams)	% Increase of lift
85 %	10050	47.78	119.18	66.92
90 %	11200	54.40	125.81	76.18
95 %	12325	58.69	130.10	82.19
100 %	13465	60.22	131.63	84.33

Similarly, for the analysis of drag force, the drag produced by the pitch rate and the elevator deflection is ignored. The

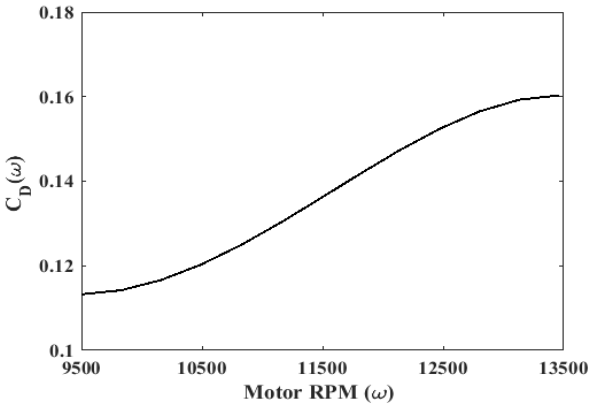

Figure 9. Drag coefficient vs Motor RPM (ω)

variation of coefficient of drag only due to propeller induced flow is shown in Figure 9, $C_D(\omega) = f_D(\omega)/(0.5\rho V_a^2 S)$.

The total coefficient of drag due to the free stream flow of 8 m/s and propeller induced flow of 11200 RPM is shown in Figure 10. At an angle of attack of 18 degree, the contribution of propeller induced flow towards total drag force at a different percentage of the throttle is shown in Table 7. The total drag force due to free stream flow of 8 m/s and propulsive flow of 11200 RPM is 50.67 grams; where propulsive flow contributed about 14.40 grams. Clearly, the propulsive flow increases the drag by 39.70 % at 90 % throttle. Therefore, the propeller induced flow has a significant effect on the total drag force.

Side force

The side force acting on the MAV mainly depends on the angle of sideslip (β), roll rate (p), yaw rate (r), aileron angle (δ_a) and asymmetric propeller flow. The side force is modelled in equation 7-8 .

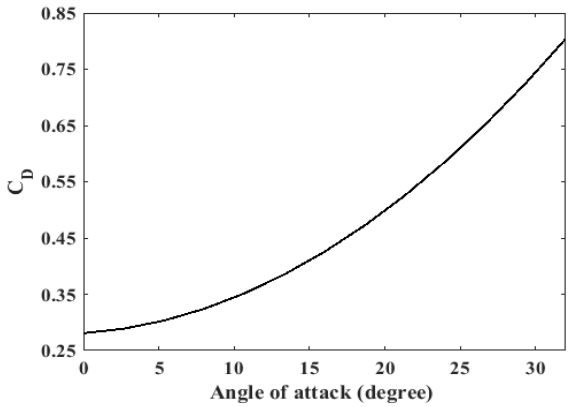

Figure 10. Total drag coefficient at 90 % throttle (Motor RPM=11200)

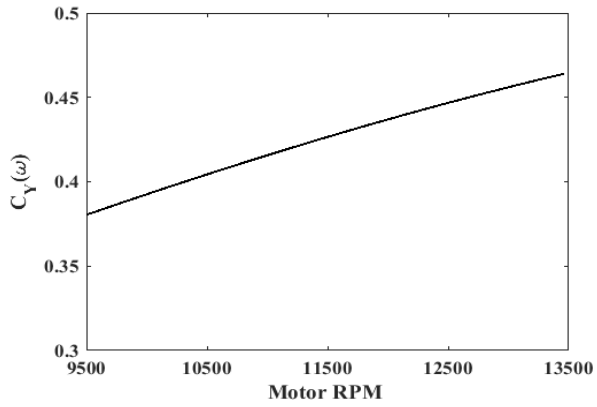

Figure 11. Side force coefficient vs Motor RPM

Table 7. Drag at different percentage of throttle.

Throttle	RPM	Drag due to propeller induced flow (grams)	Total drag (grams)	% Increase of drag
85 %	10050	12.74	49.0	35.14
90 %	11200	14.40	50.67	39.70
95 %	12325	16.55	52.81	45.64
100 %	13465	17.65	53.92	48.66

$$f_{Y_{aero}} = \frac{1}{2}\rho V_a^2 S\Big(C_Y(\beta) + C_{Y_p}\frac{b}{2V_a}p + C_{Y_r}\frac{b}{2V_a}r + C_Y(\delta_a)\Big) + f_Y(\omega) \quad (7)$$

$$f_Y(\omega) = 6.658 \times 10^{-7} - 0.4782\delta_\omega + 1.188\delta_\omega^2 - 0.639\delta_\omega^3 \quad (8)$$

where the dynamic and control derivatives terms are mentioned in Table 8.

Table 8. Side force parameter.

Parameter	value	Parameter	Value
$C_Y(\beta)$	$0.05 - 0.58\beta$	C_{Y_p}	0
C_{Y_r}	0	$C_Y(\delta_a)$	$0.1148\delta_a$

The variation of side force coefficient with the motor rotation is shown in Figure 11, here $C_Y(\omega) = f_Y(\omega)/(0.5\rho V_a^2 S)$. The increment of side force with the increase of motor rotation is due to asymmetric propeller induced flow as well as the addition of more kinetic energy to the flow.

The contribution toward the side force with respect to the angle of sideslip and aileron angle is plotted in Figure 12 and Figure 13. Clearly from Figure 11, Figure 12 and Figure 13, the relative magnitude of the lateral force generated due to motor RPM is higher than side slip angle and aileron angle. So, the propeller induced flow is the major contributing factor toward the total side force acting on the system.

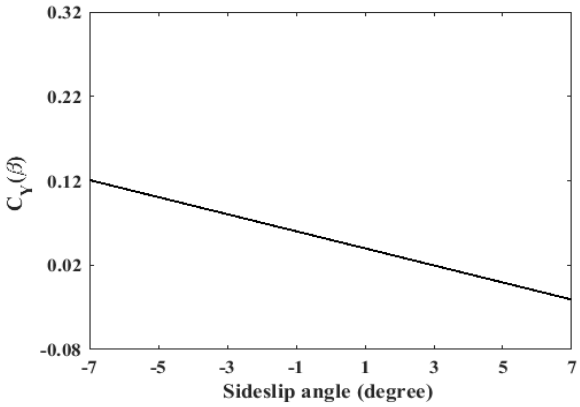

Figure 12. Contribution toward side force due to sideslip at zero aileron angle

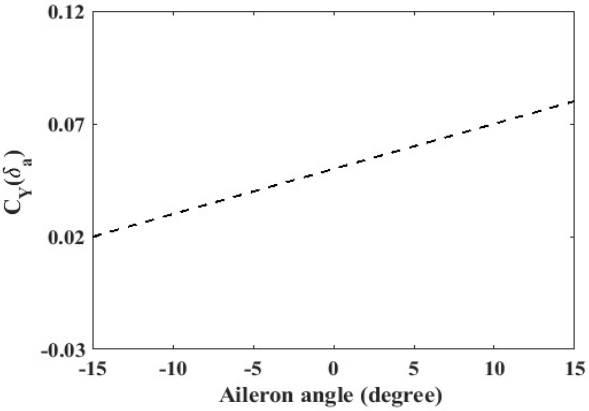

Figure 13. Contribution toward side force due to aileron at zero side slip angle

Rolling moment

The contributing factors behind the generation of the rolling moment (l) are the angle of sideslip, roll rate, pitch rate, aileron deflection, propeller induced flow and motor counter-torque. Due to the low moment of inertia of the fixed wing MAV, motor counter torque contributes to a significant part of rolling moment acting on MAV. In equation 9 and 10, expression of rolling moment (l) is given.

$$l = \frac{1}{2}\rho V_a^2 Sb\Big(C_l(\beta) + C_{l_p}\frac{b}{2V_a}p + C_{l_r}\frac{b}{2V_a}r + C_l(\delta_a)\Big) + f_l(\omega) \quad (9)$$

$$f_l(\omega) = 0.00041 + 0.05326\delta_\omega - 0.1351\delta_\omega^2 + 0.06991\delta_\omega^3 \quad (10)$$

where the rolling moment coefficients are expressed in Table 9.

Table 9. Rolling moment coefficients.

Parameter	Value	Parameter	Value
$C_l(\delta_a)$	$-0.46\beta - 0.0059$	C_{l_p}	-0.0216
C_{l_r}	0.1639	$C_l(\delta_a)$	$0.14\delta_a$

The rolling moment coefficient generated due to the propeller induced flow and motor counter-torque as a function of motor RPM is shown in Figure 14. In this case, the effect of counter-torque toward the generation of the rolling moment will have more contribution than the effect of propeller flow. The effect of counter torque is very much specific to the selected combination of motor and propeller. Neglecting the effect of roll rate, yaw rate and control surface deflection on the rolling moment; the variation of the total rolling moment coefficient as a function of the angle of sideslip at different motor rotation is shown in Figure 15. Similarly, at side slip angle of 0^o, the total rolling moment coefficient as a function of aileron deflection at different motor rotation is plotted in Figure 16. For the purpose of comparison; considering no side slip and aileron deflection of -5^o; the negative rolling moment due to propeller induced flow and motor counter-torque increases by 251 % at 100 % of throttle. It can be concluded that even after the selection of best motor-propeller combination; the moment contribution due to propeller induced flow and motor counter-torque is significant compared to aileron moment.

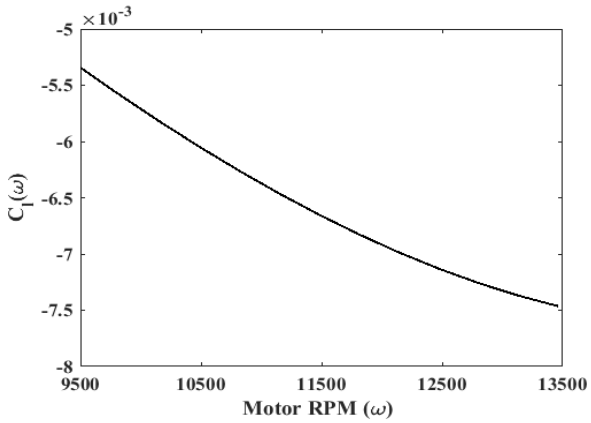

Figure 14. Rolling moment vs Motor rotation

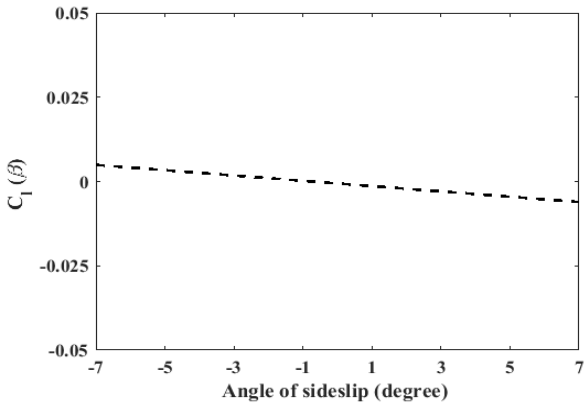

Figure 15. Contribution of sideslip angle toward rolling moment

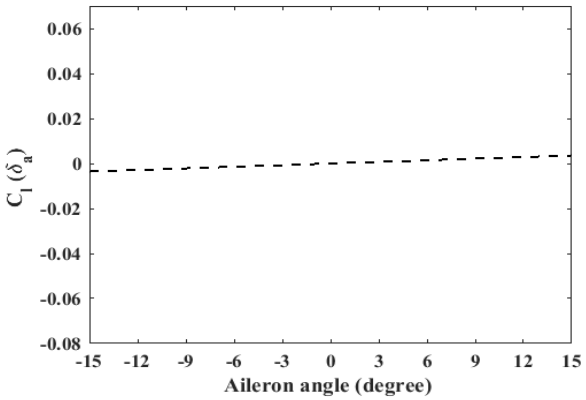

Figure 16. Contribution of aileron angle toward rolling moment

Pitching moment

Like lift and drag force, pitching moment (m) acting on the MAV depends on the angle of attack, pitch rate, elevator deflection and motor rotation. The rotation of motor generates a pitching moment as a function of thrust and propeller induced flow. In this vehicle, motor thrust axis passes through CG; hence, the pitching moment due to motor rotation will be generated only due to propeller induced flow. The pitching moment is modelled in equation 11 and 12.

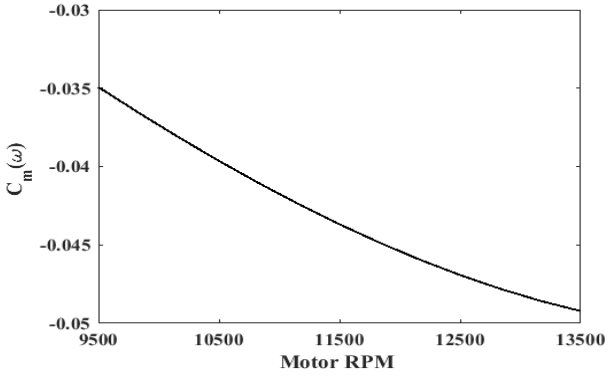

Figure 17. Pitching moment coefficient vs Motor RPM

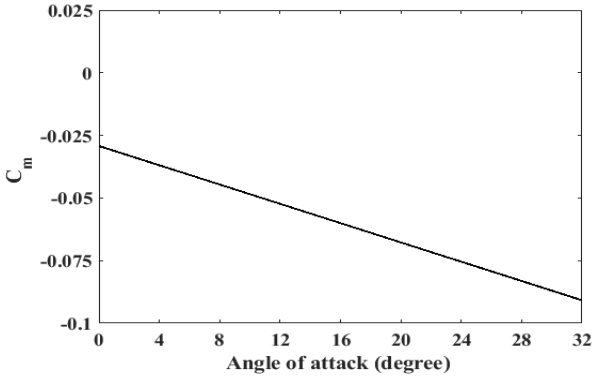

Figure 18. Pitching moment coefficient vs angle of attack

$$m = \frac{1}{2}\rho V_a^2 Sc\left(C_m(\alpha) + C_{m_q}\frac{c}{2V_a}q + C_m(\delta_e)\right) + f_m(\omega) \quad (11)$$

$$f_m(\omega) = -0.00019 + 0.33\delta_\omega - 0.8229\delta_\omega^2 + 0.4173\delta_\omega^3 \quad (12)$$

where the pitching moment coefficients are expressed in Table 10.

Table 10. Pitching moment coefficients.

Parameter	Value	Parameter	Value
$C_m(\alpha)$	$0.24 - 0.73\alpha$	$C_m(q)$	-0.2609
$C_m(\delta_e)$	$-0.5617\delta_e + 0.5703\delta_e^2$		

The variation of pitching moment coefficient as a function of motor rotation is shown in Figure 17. Figure 18 shows the total pitching moment as a function of the angle of attack at 90% throttle. Clearly, with an increase of propeller induced flow, the negative pitching moment becomes more negative. So, propeller induced flow reduces the value of the angle of attack at zero pitching moment as well as pitching moment at zero angles of attack. The angle of attack corresponding to zero pitching moment and the pitching moment at zero angles of attack affects the plant aerodynamic performance as well as longitudinal stability.

Yawing moment

The main variables which affect the rolling moment are same as the yawing moment (n). Yawing moment is modelled in equation 13 and 14.

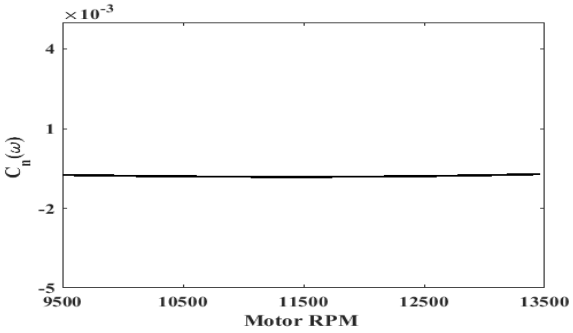

Figure 19. Yawing moment coefficient vs Motor RPM

$$n = \frac{1}{2}\rho V_a^2 Sb\left(C_n(\beta) + C_{n_p}\frac{b}{2V_a}p + C_{n_r}\frac{b}{2V_a}r + C_n(\delta_a)\right) + f_n(\omega) \quad (13)$$

$$f_n(\omega) = -0.0000997 + 0.01316\delta_\omega - 0.03349\delta_\omega^2 + 0.01925\delta_\omega^3 \quad (14)$$

where the yawing moment coefficients are expressed in Table 11.

Table 11. Yawing moment coefficients.

Parameter	Value	Parameter	Value
$C_n(\beta)$	$0.24\beta - 0.011$	C_{n_p}	0.0
C_{n_r}	-0.5375	$C_n(\delta_a)$	$0.09087\delta_a$

The variation of the yawing moment coefficient with motor rotation is shown in Figure 19. The contribution of the side slip angle toward the yawing moment coefficient is shown in Figure 20. Comparing the relative magnitude of the yawing moment from the Figure 19 and Figure 20; clearly, the propeller induced flow does not have the significant effect on the overall yawing moment.

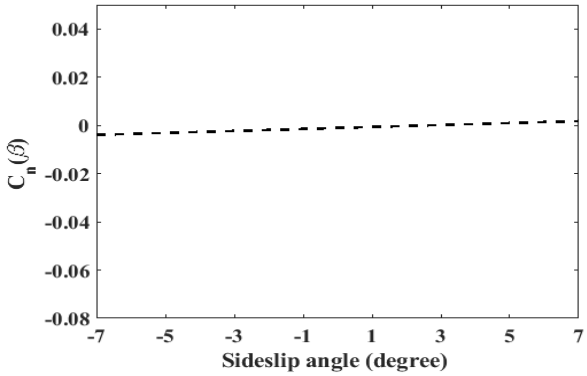

Figure 20. Contribution of side slip angle toward yawing moment

Range and endurance

The two important variables which affect the range and endurance of a vehicle are $\frac{C_L}{C_D}$ ratio and $\frac{C_L^{1.5}}{C_D}$ ratio. The range and endurance of a vehicle increases with the increase of these two parameters respectively. The $\frac{C_L}{C_D}$ ratio and $\frac{C_L^{1.5}}{C_D}$ ratio can be approximately correlated to $\frac{\text{Lift}}{\text{Drag}}$ ratio and $\frac{\text{Lift}^{1.5}}{\text{Drag}}$ ratio. The variation of $\frac{\text{Lift}}{\text{Drag}}$ as a function of angle of attack with different motor rotation is shown in Figure 21. In the case of 100 % throttle (RPM=13465) and an angle of attack of 18^o, the propulsive flow increases the $\frac{\text{Lift}}{\text{Drag}}$ ratio by 23.98 %.

Figure 22 shows the variation of $\frac{\text{Lift}^{1.5}}{\text{Drag}}$ with angle of attack at different motor rotation. At 100 % (RPM=13465) throttle and angle of attack of 18^o, the propulsive flow increases the parameter $\frac{\text{Lift}^{1.5}}{\text{Drag}}$ by 68.26 %. Clearly from the Figure 21 and Figure 22, propeller induced flow have positive effect on the range and endurance of the vehicle after a certain threshold of motor RPM.

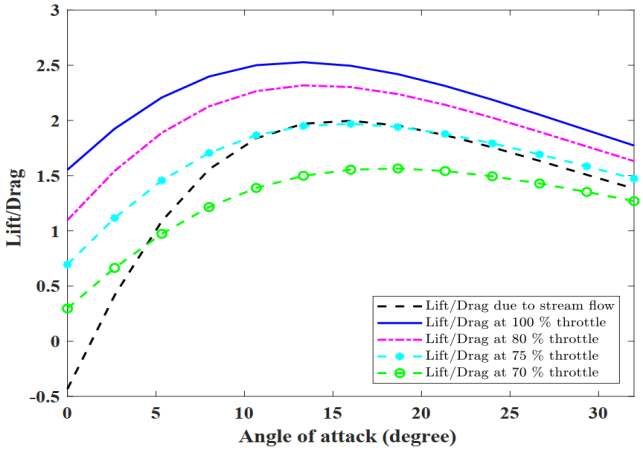

Figure 21. Contribution toward $\frac{\text{Lift}}{\text{Drag}}$ due to propeller induced flow at different RPM

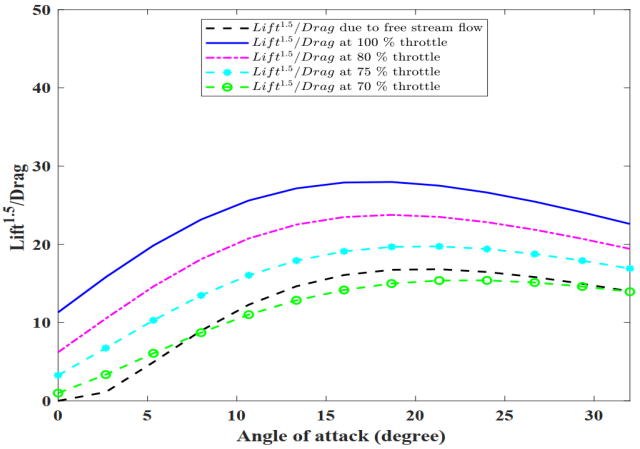

Figure 22. Contribution toward $\frac{Lift^{1.5}}{Drag}$ due to propeller induced flow at different RPM

Trim point analysis

The trim point analysis of the non-linear model of the vehicle is performed with and without propulsive flow. The equilibrium value of the different states and control variables for steady and constant turning flight of radius 25 m, at the operating point for the nominal velocity of 8 m/s with and without propulsive flow, are tabulated in Table 12 with both the cases. The state variables are velocity (u, v, w), attitude (ϕ, θ, ψ), and attitude rates (p, q, r); whereas control variables are elevator (δ_e), aileron (δ_a), and throttle (δ_ω). The unit of velocity is in m/s, the attitude in degrees, attitude rate in degrees/s and control variables are in degrees.

Table 12. Variation of trim point.

Variable	Without propeller induced flow	With propeller induced flow
u	7.34	7.66
v	0.11	-0.09
w	3.21	2.34
ϕ	-2.45	-5.56
θ	23.58	16.91
ψ	0	0
p	-0.37	-0.27
q	-0.03	-0.09
r	0.84	0.87
δ_e	-5.65	-13.64
δ_a	4.95	11.43
δ_ω	0.68	0.70

comparing the trim values of the state variables in the case of propeller induced flow with no propeller induced flow; clearly, trim values varies significantly due to propeller induced flow. The contribution of propeller induced flow to the overall forces and moments at the trim point are tabulated in Table 13.

Table 13. Contribution of propeller flow at trim point.

Quantity	Total	Contribution due to propeller induced flow	% Contribution of propeller induced flow
Lift force (grams)	61.64	17.87	28.99 %
Drag force (grams)	58.19	21.30	36.60 %
Side force (N)	0.33	0.40	81.57 %
Pitching moment (N-m)	0.0244	-0.0045	-18.34 %

Results

Clearly, many of the aerodynamic parameters are significantly affected by the propeller flow. From Table 6 and 7, at RPM of 13465 (100 % throttle), lift coefficient and drag coefficient are found to be increased by 84.33 % and 48.66 % due to propulsive flow. At same RPM of 13465 and at an angle of attack of 18^o, propulsive flow increases $\frac{C_L}{C_D}$ ratio and $\frac{C_L^{1.5}}{C_D}$ ratio by 23.98 % and 68.26 % respectively. Similarly, the combined effect of propeller induced flow and motor countertorque increases the negative rolling moment by 251 %. Propulsive flow affects the pitching moment by 40 %; whereas, the yawing moment remains unaffected. From Table 12, it is clear that there is also a significant variation of aerodynamic states due to propulsive flow. Specifically, it reduces the trim angle of attack but increases the trim roll angle.

Discussions

The effect of propeller induced flow on the MAV system dynamics is highly specific to the particular MAV configuration. However, a general conclusion can be drawn regarding the effect of propeller induced flow on MAV. The major points are as follows:

- Lift force: The amount of produced lift increases with the propulsive flow.
- Drag force: The total amount of drag produced by the combined effect of propeller induced flow and free stream flow is higher than the drag produced due to free stream flow, and it increases with motor RPM.
- Side force: Side force increases with the increase in the propulsive flow; however, its amount is highly dependent on the size of the vertical surface in the slipstream.
- Moments: The magnitude of the rolling moment and pitching moment increases with the propeller induced flow. In case of rolling moment, motor counter torque contributes a major part of additional moment. Effect on yawing moment due to propeller induced flow is less.
- The range and endurance of the vehicle are significantly affected due to propeller rotation; and after a threshold RPM, range and endurance of a vehicle increase with the propeller induced flow.

Conclusions

Modelling and analysis of propeller induced flow on the dynamics of a fixed-wing biplane MAV are presented. The effect of propeller flow is modelled as a function of motor rotation from the wind tunnel test data. For a typical constant turning flight condition, the effect of propeller rotation approximately increased 28.99 % of lift force, 36.60 % of drag force, 81.57 % of side force. Rolling and pitching are also being affected by a significant amount. Propeller induced flow reduced the trim angle of attack and it further reduced with the increase of rotation rate. Range and endurance increases with propeller induced flow. Clearly, the propeller rotation plays a crucial role in aerodynamic performance and efficiency of MAV and its accurate modelling is important for system design. The analysis in this paper will help in the design of MAV configuration.

Acknowledgements

The authors would like to thank National Aerospace Laboratory (NAL) for allowing us to conduct wind tunnel test. The authors would also like to thank Shashank Shivkumar, Susheel Balasubramaniam, Eshaan Khanapuri, Kuntal Ghosh for helping us in conducting wind tunnel test and flow simulation.

Declaration of conflicting interests

The author(s) declared no potential conflicts of interest with respect to the research, authorship, and/or publication of this article.

Funding

The work is funded under National Programme for Micro Air Vehicle (NP-MICAV) project of Defence Research Development Organization (DRDO). The authors would like to thank Aeronautics Research and Development Board (ARDB) for their funding and support for the project.

References

1.Hassanalian M, Khaki H and Khosravi M. A new method for design of fixed wing micro air vehicle. *Proceedings of the Institution of Mechanical Engineers, Part G: Journal of Aerospace Engineering* 2015; 229(5): 837–850.

2.McMichael JM and Francis MS. Micro air vehicles-toward a new dimension in flight. *DARPA document* 1997; .

3.Brenckmann ME. Experimental investigation of the aerodynamics of a wing in a slipstream. *Journal of the Aerospace Sciences* 1958; 25(5): 324–328.

4.George M and Kisielowski E. Investigation of propeller slipstream effects on wing performance. Technical report, Dynasciences Corp Blue Bell PA, 1967.

5.Witkowski DP, Lee AK and Sullivan JP. Aerodynamic interaction between propellers and wings. *Journal of Aircraft* 1989; 26(9): 829–836.

6.Catalano F. On the effects of an installed propeller slipstream on wing aerodynamic characteristics. *Acta Polytechnica* 2004; 44(3).

7.Veldhuis LLM. *Propeller wing aerodynamic interference*. PhD Thesis, TU Delft, Delft University of Technology, 2005.

8.Shyy W, Lian Y, Tang J et al. *Aerodynamics of low Reynolds number flyers*, volume 22. Cambridge University Press, 2007.

9.Aminaei H, Dehghan Manshadi M and Mostofizadeh AR. Experimental investigation of propeller slipstream effects on the wing aerodynamics and boundary layer treatment at low Reynolds number. *Proceedings of the Institution of Mechanical Engineers, Part G: Journal of Aerospace Engineering* 2018; DOI:10.1177/0954410018793703.

10.Chinwicharnam K and Thipyopas C. Comparison of wing–propeller interaction in tractor and pusher configuration. *International Journal of Micro Air Vehicles* 2016; 8(1): 3–20.

11.Arivoli D, Dodamani R, Antony R et al. Experimental studies on a propelled micro air vehicle. In *Proceedings of the 29th AIAA Applied Aerodynamics Conference, No. AIAA*, Honolulu, Hawaii, 27-30 June 2011, volume 3656.

12.Durai A. Experimental investigation of lift and drag characteristics of a typical mav under propeller induced flow. *International Journal of Micro Air Vehicles* 2014; 6(1): 63–72.

13.Ananda GK, Deters RW and Selig MS. Propeller-induced flow effects on wings of varying aspect ratio at low reynolds numbers. *AIAA Paper* 2014; 2014–2152.

14.Ananda Krishnan GK, Deters RW and Selig MS. Propeller induced flow effects on wings at low Reynolds numbers. In *31st AIAA Applied Aerodynamics Conference*, San Diego, CA, 24-27 June 2013, p. 3193.

15.Null W, Noscek A and Shkarayev S. Effects of propulsive-induced flow on the aerodynamics of micro air vehicles. In *23rd AIAA Applied Aerodynamics Conference*, Toronto, Canada, 6-9 June 2005, p. 4616.

16.Ananda GK, Selig MS and Deters RW. Experiments of propeller-induced flow effects on a low-reynolds-number wing. *AIAA Journal* 2018; 56(8): 3279–3294.

17.Ahn J and Lee D. Aerodynamic characteristics of a micro air vehicle and the influence of propeller location. In *31st AIAA Applied Aerodynamics Conference*, San Diego, CA, 24-27 June 2013, p. 2655.

18.Choi S and Ahn J. A computational study on the aerodynamic influence of a pusher propeller on a mav. In *40th Fluid Dynamics Conference and Exhibit*, 2010, p. 4741.

19.Bakkhoshnevis A, Mamouri AR and Khodadadi S. Experimental investigation for wake of the circular cylinder by attaching different number of tripping wires. *Iranian Journal of Mechanical Engineering Transactions of the ISME* 2016; 17, 525.

20.Bakkhoshnevis A, Mamouri AR and Nazari M. Experimental investigation of wake on an elliptic cylinder in the presence of tripping wire. *Iranian Journal of Mechanical Engineering Transactions of the ISME* 2017; 18, 81102.

21.Ageev N. Numerical investigation of disc-wing mav with propeller in a wing slot. *In International Micro Air Vehicle conference and competitions 2011 (IMAV 2011)*, 't Harde, Netherlands 2011.

22.Deng S, W van Oudheusden B, Xiao T et al. A computational study on the aerodynamic influence of a propeller on an mav by unstructured overset grid technique and low mach number preconditioning. *The Open Aerospace Engineering Journal* 2012; 5(1).

23.Khan W, Nahon M and Caverly R. Propeller slipstream model for small unmanned aerial vehicles. In *AIAA Modeling and Simulation Technologies (MST) Conference*, Boston, MA, 19-22 August 2013, p. 4907.

24.Sharpe P and Agarwal RK. Conceptual and numerical analysis of active wingtip vortex cancellation in propeller-driven electric aircraft. In *AIAA Scitech 2019 Forum*, 2019, p. 1091.

25.Randall R, Hoffmann CA and Shkarayev S. Longitudinal aerodynamics of a vertical takeoff and landing micro air vehicle. *Journal of Aircraft* 2011; 48(1): 166–176.

26.Sudhakar S, Kumar C, Arivoli D et al. Experimental studies of propeller induced flow over a typical micro air vehicle. *AIAA Paper* 2013; 60.

27.Sharma P and Atkins EM. An experimental investigation of tractor and pusher hexacopter performance. In *2018 Atmospheric Flight Mechanics Conference*, Atlanta, USA, 25-29 June 2018, p. 2983.

28.Khoshnevis AB, Barzenoni V and Mamouri AR. Experimental study of parameters and high-order values of velocity in the behind wake of a vehicle model. *International Journal of Automotive Engineering* 2016; 6(4): 2291–2300.

29.Spoerry MT and Wong K. Design and development of a micro air vehicle (μav) concept: Project bidule. In *The 9th Annual International Aerospace Congress. School of Aerospace, Mechanical and Mechatronic Engineering, University of Sydney, NSW, Australia*, 2011.

30.Harikumar K, Dhall S and Bhat MS. Nonlinear modeling and control of coupled dynamics of a fixed wing micro air vehicle. In *Control Conference (ICC), 2016 Indian*. IEEE, pp. 318–323.

31.Thipyopas C and Moschetta J. A fixed-wing biplane MAV for low speed missions. *International Journal of Micro Air Vehicles* 2009; 1(1): 13–33.

32.Jana S. *Novel Biplane Micro Air Vehicle System with Adaptive Control and Vision Augmentation*. PhD Thesis, Indian Institute of Science; Bengaluru, 2018.

33.Roskam J. *Airplane Design*, volume 6. Roskam aviation and engineering corporation, 1990.